Check for updates

A novel macroporous polymer–inorganic nanocomposite as a sorbent for pertechnetate ions

Bojana M. Marković,[a] Drina Lj. Janković,[b] Aleksandar A. Vukadinović,[b] Danijela V. Ranđelović,[a] Danijela D. Maksin,[b] Vojislav V. Spasojević[b] and Aleksandra B. Nastasović [ID] *[a]

A novel magnetic macroporous poly(glycidyl methacrylate-*co*-ethylene glycol dimethacrylate) (mPGME) was prepared by suspension copolymerization and functionalized with diethylenetriamine (mPGME-deta). The samples were characterized by Fourier transform infrared spectroscopy (FTIR) analysis, mercury porosimetry, scanning electron microscopy with energy-dispersive X-ray spectroscopy (SEM-EDS), atomic force microscopy (AFM) and SQUID magnetometry. The sorption behavior of mPGME-deta toward pertechnetate ions (TcO_4^-) from aqueous solution was studied. Experimental results indicated relatively fast TcO_4^- sorption kinetics that depends on pH and ionic strength, with a high removal efficiency of 99% within 180 min in the pH range 3.0–5.0. The pseudo-second-order model yielded the best fit for the kinetic data.

Introduction

Technetium-99 (^{99}Tc) is a soft β-emitter ($E_{\beta max} = 294$ keV) and a high yield (6%) fission product of uranium-235 (^{235}U) and plutonium-239 (^{239}Pu) with a long half-life (2.11×10^5 years) and long-term radiological effects.[1] In a reducing environment, Tc is present in the +4 state, forming soluble hydroxides $TcO_2 \cdot nH_2O$, while, under oxidizing conditions, the predominant form of Tc is the pertechnetate oxyanion (TcO_4^-) which is highly soluble and difficult to eliminate, posing a significant environmental hazard.[2,3]

Several polymeric sorbents have been investigated for their potential use in pertechnetate removal, like commercial anion-exchange resins,[4] bifunctional chloromethylstyrene based anion-exchange resins cross-linked with divinylbenzene (DVB) with quaternary ammonium groups (triethylamine and trihexylamine),[5] noncovalently immobilized (thia)calix[4]arenes on Amberlite XAD-7,[6] 4-vinylpyridine-based resins,[7] *etc.*

Magnetic polymers are composed of a magnetic (Fe_3O_4, Fe_2O_3, nickel and cobalt) and polymer component that can be easily manipulated with a magnetic field. So far these types of materials have been used in catalysis, biotechnology/biomedicine, magnetic resonance imaging,[8] metal chelation,[9] *etc.* Magnetic polymers can be prepared from separately obtained polymers and magnetic cores (phase-separation, solvent evaporation and layer-by-layer process), or *in situ* by polymerization in a continuous phase in the presence of inorganic particles by suspension,

dispersion, emulsion, miniemulsion, and microemulsion polymerization. Various preparation methods provide magnetic polymer microspheres with different morphology, like magnetic core–polymer shell, magnetic multicores homogeneously dispersed within the polymer matrix, polymer core coated magnetic nanoparticles ("strawberry" morphology) and polymer chains attached to the magnetic core ("brush" morphology).[10] The most important parameters for application of magnetic copolymers are the size, size distribution, morphology, hydrophobicity/hydrophilicity, density of reactive surface groups and magnetic properties.[11]

Our previous studies have shown that PGME-deta due to the presence of numerous functional groups (–OH and –NH$_2$) can be used for binding of metal oxo-anion species, like Cr and Mo.[12–14] The sorption ability of PGME-deta towards pertechnetate anions was also investigated.[15,16] In this study, magnetic macroporous poly(glycidyl methacrylate-*co*-ethylene glycol dimethacrylate) copolymer (mPGME) was prepared by suspension polymerization, functionalized with diethylenetriamine (mPGME-deta) and tested as a potential technetium-99 sorbent in form of pertechnetate ion (TcO_4^-) from aqueous solutions. The morphology, chemical and physical properties of mPGME and mPGME-deta were evaluated using Fourier transform infrared spectroscopy (FTIR) analysis, mercury porosimetry, scanning electron microscopy with energy-dispersive X-ray spectroscopy (SEM-EDS), atomic force microscopy (AFM) and SQUID magnetometry.

To the best of our knowledge, the study regarding the TcO_4^- sorption onto mPGME has not been published. Thus, basic objectives of this study were to study the effect of various experimental parameters such as the contact time, sample pH, competing anions and ionic strength on the sorption of pertechnetate anions by mPGME-deta as well to investigate the

[a]Institute of Chemistry Technology and Metallurgy, University of Belgrade, Njegoševa 12, Belgrade, Republic of Serbia. E-mail: anastaso@chem.bg.ac.rs; anastasovic@gmail.com; Fax: +381 11 2636 061; Tel: +381 11 2635 839

[b]Vinča Institute of Nuclear Sciences, University of Belgrade, P. O. Box 522, 11001 Belgrade, Republic of Serbia

kinetics and equilibrium isotherms. Surface-reaction (pseudo-first-order, PFO and pseudo-second-order, PSO) and particle diffusion-based (intraparticle diffusion, IPD and Boyd's) kinetic models were used for analysis of the kinetic data. Adsorption isotherms were studied at varying pertechnetate concentrations and different background solutions.

Experimental section

Materials

Glycidyl methacrylate (GMA), diethylene triamine, 2,2′-azobisiso-butyronitrile, (AIBN), cyclohexanol and 1-tetradecanol were purchased from Merck (Germany). Ethylene glycol dimethacrylate (EGDMA) was supplied from Fluka (USA). Poly(N-vinyl pyrrolidone) (PVP, Kollidone 90) was purchased from BASF (Germany). $FeSO_4 \cdot 7H_2O$ and $FeCl_3 \cdot 6H_2O$ (Sigma-Aldrich) were used as sources for Fe(II) and Fe(III). All the other chemicals were analytical grade reagents. Technetium ($^{99m}Tc + ^{99}Tc$) was eluted from $^{99}Mo/^{99m}Tc$ generator (Vinča Institute of Nuclear Sciences, Belgrade, Serbia) in the form of sodium pertechnetate using normal saline (0.9% NaCl). The specific activity of ^{99m}Tc in sodium pertechnetate solution was determined by a Capintec CRC-15beta dose calibrator. Both ^{99}Tc and ^{99m}Tc were contained in the pertechnetate form. A pH meter, Beckman F40 with a combined Ag/AgCl electrode, was employed for adjusting pH values. Adsorption isotherms of pertechnetate ($^{99}TcO_4^- + ^{99m}TcO4^-$) by the mPGME-deta was carried out in various background solutions including deionized water (Milli-Q Millipore 18 MΩ cm^{-1} conductivity), 0.01 M KNO_3, 0.1 M KNO_3, 1 M KNO_3 and groundwater from Bukulja mountain near Arandjelovac town (Republic of Serbia). The groundwater chemistry is provided in Table 1. Purified deionized water used in all experiments was prepared by the Milli-Q system (Millipore Co., Billerica, MA, USA).

Synthesis of magnetite nanoparticles

Superparamagnetic magnetite nanoparticles were prepared *via* improved chemical co-precipitation method.[17] According to this method, 0.016 mol of $FeSO_4 \cdot 7H_2O$ and 0.028 mol of $FeCl_3 \cdot 6H_2O$ were dissolved in 320 ml of deionized water, stirred under N_2 at 80 °C. After 1 h, 40 ml of $NH_3 \cdot H_2O$ solution was injected rapidly into the mixture (at pH ∼ 10), stirred for another 1 h and cooled to room temperature. The precipitated magnetic particles were washed five times with hot water, separated by magnetic decantation and dried under vacuum at 70 °C.

mPGME synthesis and amino-functionalization

Macroporous mPGME copolymer was prepared by suspension copolymerization of glycidyl methacrylate (GMA) and ethylene glycol dimethacrylate (EGDMA, crosslinker), in the presence of inert component and suspended magnetite nanoparticles (2 mass%). The aqueous phase consisting of 225.0 g of water and 2.25 g poly(N-vinyl pyrrolidone) was placed in polymerization reactor and heated to 70 °C. The monomer phase containing monomer mixture (19.5 g GMA and 29.1 g EGDMA), AIBN as initiator (0.5 g), 63.8 g of inert component (51.0 g of cyclohexanol and 12.8 g of tetradecanol) and 1.45 g of magnetite (Fe_3O_4) nanoparticles was sonicated for 30 min at 300/600 W within an ultrasonic water bath (Sonic 12GT). The resulting mixture was dropped into polymerization reactor. The reaction mixture was stirred at 300 rpm during the monomer addition and heating was started. The copolymerization was carried out under nitrogen atmosphere at 75 °C for 2 h and at 80 °C for 2 h with a stirring rate of 250 rpm. After the reaction mPGME was washed with water and ethanol, kept in ethanol for 12 h, and dried in vacuum at 50 °C. Particles with average particle diameter (D) in the range 150–300 μm were used for subsequent functionalization with diethylene triamine as described elsewhere.[18] A mixture of 3.6 g of mPGME, 15.7 g of diethylene triamine, and 100 cm^3 of toluene was left at room temperature for 24 h and then heated at 80 °C for 6 h. The amino-functionalized sample was filtered, washed with ethanol, dried, and labeled as mPGME-deta.

mPGME and mPGME-deta characterization

The pore size distribution was determined by mercury porosimetry (Carlo Erba 2000, software Milestone 200). Fourier transform infrared (FTIR) spectra were recorded using a Nicolet 380 spectrometer equipped with a Smart Orbit™ ATR attachment containing a single-reflection diamond crystal. The scanning electron microscopy (SEM) micrographs were obtained on JEOL JSM-6460LV instrument (Tokyo, Japan), at a working distance of *ca.* 14 mm and an accelerating voltage of 20 kV. Functionalized samples were coated with gold in a high-vacuum evaporator. The energy dispersive spectroscopic (EDS) analysis was performed on Jeol JSM 5800 instrument operating at 20 kV. AFM characterizations were performed with AutoProbe CP-Research SPM (TM Microscopes-Veeco) using 90 μm large area scanner. Measurements were carried out in air using non-contact AFM mode, at the scan size (2 × 2) μm^2 with the resolution of (256 × 256) data points per image. AFM images were created and analysed using two software packages Image Processing and Data Analysis Version 2.1.15 and SPMLab Analysis software, VEECO DI SPMLab NT Ver. 6.0.2. The roughness analysis was performed using Image Analysis 2.1.2 software, while fractal analysis was performed by partitioning method implementing Fractal Dimension tool available within freeware Gwyddion 2.43. Field dependence of isothermal magnetization $M(H)$ at room temperature was measured on a SQUID-based

Table 1 Chemical properties of groundwater used in adsorption studies

Ion	mg l^{-1}
Calcium (Ca^{2+})	83
Magnesium (Mg^{2+})	19
Sodium (Na^+)	9.9
Potassium (K^+)	1.6
Iron ($Fe^{2+/3+}$)	<0.05
Bicarbonate (HCO_3^-)	317
Sulfate (SO_4^{2-})	21.2
Chloride (Cl^-)	11.5
Fluoride (F^-)	0.18

commercial magnetometer Quantum Design MPMS-XL-5, in the applied DC fields up to 5 T.

For determination of the amino groups content, 100 mg of mPGME-deta was immersed in 5.2 cm³ 0.1 M HCl solution for 24 hours. After this period 2 cm³ of the solution was taken and the excess of acid was titrated with 0.052 M NaOH in the presence of phenolphthalein solution until the solution turned violet.[19] The content of amino groups, C_{AG} (mmol g⁻¹) was calculated from:

$$C_{AG} = \frac{(C_1 V_1 - 2 C_2 V_2)}{m} \qquad (1)$$

where: C_1 is the initial HCl concentration (0.105 M), V_1 is the initial volume of the HCl solution (5.2 cm³), C_2 is the concentration of the NaOH solution (0.052 M), V_2 is the volume of the NaOH solution used for the titration, and m is the mass of the copolymer sample. The amino group concentration (C_{AG}) of mPGME-deta value obtained by titration was 3.55 mmol g⁻¹.

The point of zero charge (pH$_{pzc}$ value) of mPGME-deta was determined by the pH drift method.[20] The initial pH (pH$_i$) of test solutions (20 cm³ of 0.01 M NaCl in a series of Erlenmeyer flasks) was adjusted in the pH range between 2 and 12 by adding NaOH or HCl. After that, 50.0 mg of the mPGME-deta was added in the flasks and the final pH values of the solutions (pH$_f$) were measured after 24 h. The pH at which the curve crosses pH$_i$ = pH$_f$ line was taken as pH$_{pzc}$.[21] pH was measured by Hanna HI 2210 pH meter calibrated before every measure.

Pertechnetate ions sorption onto mPGME-deta

The effect of contact time and pH was studied by shaking (at 120 rpm) 1 mg of mPGME-deta with 4.9 cm³ of the buffer solution and 0.1 ml of TcO$_4^-$ solution in 10 cm³ borosilicate glass vials. The effect of pH on the TcO$_4^-$ adsorption on PGME-deta and mPGME-deta was investigated in aqueous buffer solutions in a pH range 1–8. The blanks without copolymer were prepared in the same manner. For sorption isotherms determination, the concentration of TcO$_4^-$ was in the range 0.2–500 pmol ml⁻¹, while the pH was 5.0 ± 0.5, i.e. in the range of favorable pH. The solutions were equilibrated for 48 h.

All uptake experiments were conducted in triplicate. In predetermined time intervals, 100 μl aliquots from the vials containing mPGME-deta as well as from the blanks were taken. The aliquot activity was measured in well-type NaI (Tl) gamma counter (2480 WIZARD Automatic Gamma Counter, Perkin Elmer, USA).

Data treatment

The exact values for the amount of ⁹⁹ᵐTc and ⁹⁹Tc in sodium pertechnetate solution, obtained by eluting the ⁹⁹Mo/⁹⁹ᵐTc generator, can be calculated using the equations derived for the generator kinetics of the parent–daughter relationship.[22,23]

The amount of ⁹⁹ᵐTc and ⁹⁹Tc (pmol) in supernatant and the amount of adsorbed ⁹⁹ᵐTc and ⁹⁹Tc were calculated based on the total number of technetium atoms (⁹⁹Tc and ⁹⁹ᵐTc) per mCi.

Relative measurements of adsorbed radioactivity were obtained using the following eqn (2):

$$R = \frac{R_b - R_s}{R_b} \times 100\% \qquad (2)$$

where R is the adsorbed ⁹⁹ᵐTc activity (%), R_b is the measured activity of the blank aliquot (counts per min) and R_s is the activity of the supernatant aliquot from the vials containing polymer (counts per min).

The partition coefficients, K_d (ml g⁻¹), were calculated according to the eqn (3):

$$K_d = \frac{S}{C} \qquad (3)$$

where S represents the adsorbed concentration on adsorbent surface, expressed as the amount (in pmoles) of technetium (⁹⁹Tc + ⁹⁹ᵐTc) per gram of solid and C is the equilibrium aqueous concentration of technetium (⁹⁹Tc + ⁹⁹ᵐTc) (pmol per ml of solution).

Kinetics analysis

The data for pertechnetate ion sorption by mPGME-deta were analyzed using pseudo-first order (PFO), pseudo-second order (PSO), intraparticle diffusion (IPD) and Boyd's kinetic models.

The linearized form of PFO (eqn (4)) and PSO (eqn (5))[24] kinetic models used for calculations were as follows:

$$\log(q_e - q_t) = \log q_e - \frac{k_1 t}{2.303} \qquad (4)$$

$$\frac{t}{q_t} = \frac{1}{k_2 q_e^2} + \frac{1}{q_e} t \qquad (5)$$

where: q_e (MBq g⁻¹) is the amount of sorbed technetium at equilibrium; k_1 (min⁻¹) is the PFO rate constant; k_2 (g MBq⁻¹ min⁻¹) is the PSO rate constant.

The corresponding equations for intraparticle (IPD) (eqn (6)) and Boyd's (eqn (7))[25] kinetic models were as follows:

$$q_t = k_d t^{1/2} + c \qquad (6)$$

$$B_t = -0.4997 - \ln(1 - G) \qquad (7)$$

where k_d (MBq g⁻¹ min⁻⁰·⁵) is the intraparticle diffusion coefficient; c (MBq g⁻¹) is a constant, related to the thickness of the boundary layer; B_t is a mathematical function of G; G is the fractional attainment of equilibrium at time t, calculated as: $G = q_t/q_e$.

Results and discussion

Characterization of mPGME and mPGME-deta

The synthesized magnetic mPGME sample was sieved with 0.15, 0.30 and 0.63 mm sieves. The results of sieve analysis were compared with non-magnetic sample PGME and presented in Fig. 1.

As can be seen, the particle fraction with diameter in 0.15–0.30 mm range is highly dominant for sample mPGME, approximately 95 mass%. It appears that the addition of magnetite in the reaction mixture considerably influences the formation of macroporous structure, narrows the size
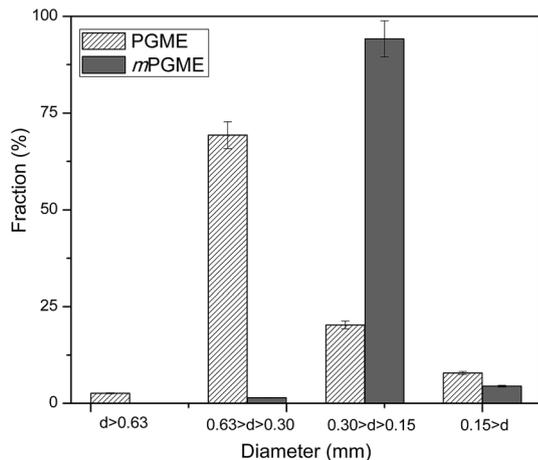
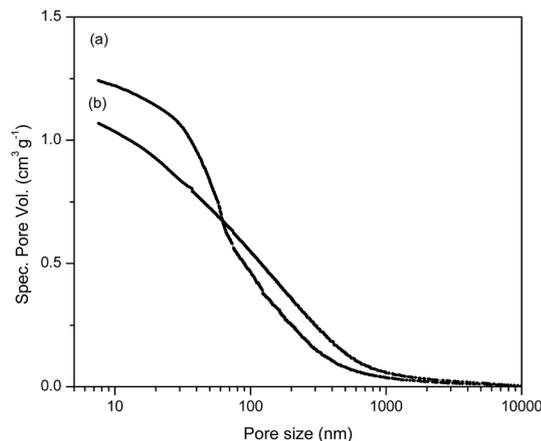Fig. 1 Sieve analysis of non-magnetic and magnetic copolymer samples.

Fig. 2 Cumulative pore volume distribution curves for (a) mPGME-deta and (b) mPGME.

distribution and shifts it to the smaller particles in comparison with PGME synthesis. We previously observed the similar for PGME/bentonite composites.[26]

The cumulative pore volume distribution curves for selected samples are presented in Fig. 2. The relevant porosity parameters (specific pore volume, V_S, specific surface area, S_{Hg}, and pore diameter that corresponds to half of the pore volume, $D_{V/2}$) for mPGME and mPGME-deta were calculated from the cumulative pore volume distribution curves as described in the literature[27] and presented in Table 2.

It can be seen from porosity data that the amino-functionalization alters the porous structure of magnetic

Table 2 Porosity parameters of mPGME and mPGME-deta

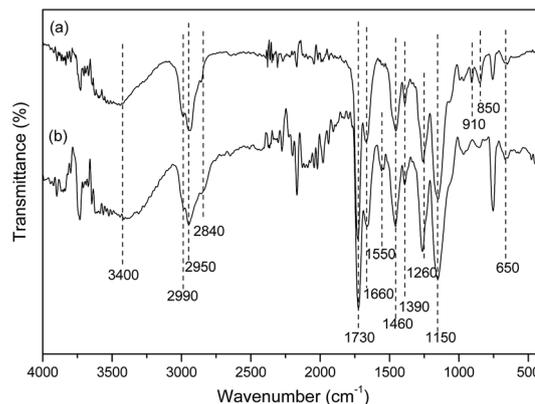| Copolymer sample	$S_{s,Hg}$, m² g⁻¹	V_s, cm³ g⁻¹	$D_{V/2}$, nm
mPGME	92	1.07	102
mPGME-deta	100	1.24	66

Fig. 3 FTIR spectra of (a) mPGME and (b) mPGME-deta.

copolymer, causing a shift in the pore size distribution curves of the synthesized samples towards higher specific pore volume and smaller pores, i.e. sample mPGME-deta has almost twice lower $D_{V/2}$ value. However, the influence of amino-functionalization on S_{Hg} value is negligible.

The FTIR spectra of mPGME and mPGME-deta were recorded and presented in Fig. 3.

In the FTIR spectra of magnetic copolymer samples the characteristic absorption bands at ~2990 cm⁻¹, ~2950 cm⁻¹ and ~2840 cm⁻¹ (methyl and methylene stretching vibrations, $\nu_{C–H}$), ~1730 cm⁻¹ (ester carbonyl vibrations, $\nu_{C=O}$), ~1390 and ~1460 cm⁻¹ (methyl and methylene bending vibrations, $\delta_{C–Hasym}$ and $\delta_{C–Hsym}$) were observed. Also, the characteristic peaks for epoxy ring vibrations at ~850 and ~910 cm⁻¹ and 1260 cm⁻¹ (stretching vibrations, $\nu_{C–O}$) and ~1150 cm⁻¹ (ether stretching vibrations, $\nu_{C–O–C}$) were found in the mPGME spectrum.[28] The characteristic stretching frequencies of the amino-functionalized sample mPGME-deta appeared at 1550 cm⁻¹ (δ_{NH}).

The FTIR spectra for both samples confirm the incorporation of magnetite in the macroporous PGME. Namely, the bands in the 650–575 cm⁻¹ range could be attributed to the vibrations of Fe–O bonds in tetrahedral and octahedral sites.[29,30] According to the literature, the band at ~420 cm⁻¹ originates from octahedral Fe and corresponds to the band of Fe–O of bulk magnetite (~370 cm⁻¹) shifted to a higher wavenumber. The presence of O–H stretching vibration at ~3400 cm⁻¹ and O–H bending vibrations at 1660 cm⁻¹ could be ascribed to the presence of coordinated OH groups or water molecules with the unsaturated surface Fe atoms.[30]

For further analysis, the morphology of mPGME and mPGME-deta samples was examined by SEM with energy-dispersive X-ray spectroscopy (SEM-EDS). The results were presented in Fig. 4 and Table 3.

The micrographs demonstrate three dimensional porous structures of the samples, composed of a large number of globules and interconnected with channels and pores. Also, from Fig. 4 it is visible that the iron particles are dispersed on the surface of mPGME and mPGME-deta particles. The similar was observed for crosslinked ionic polymers containing strongly
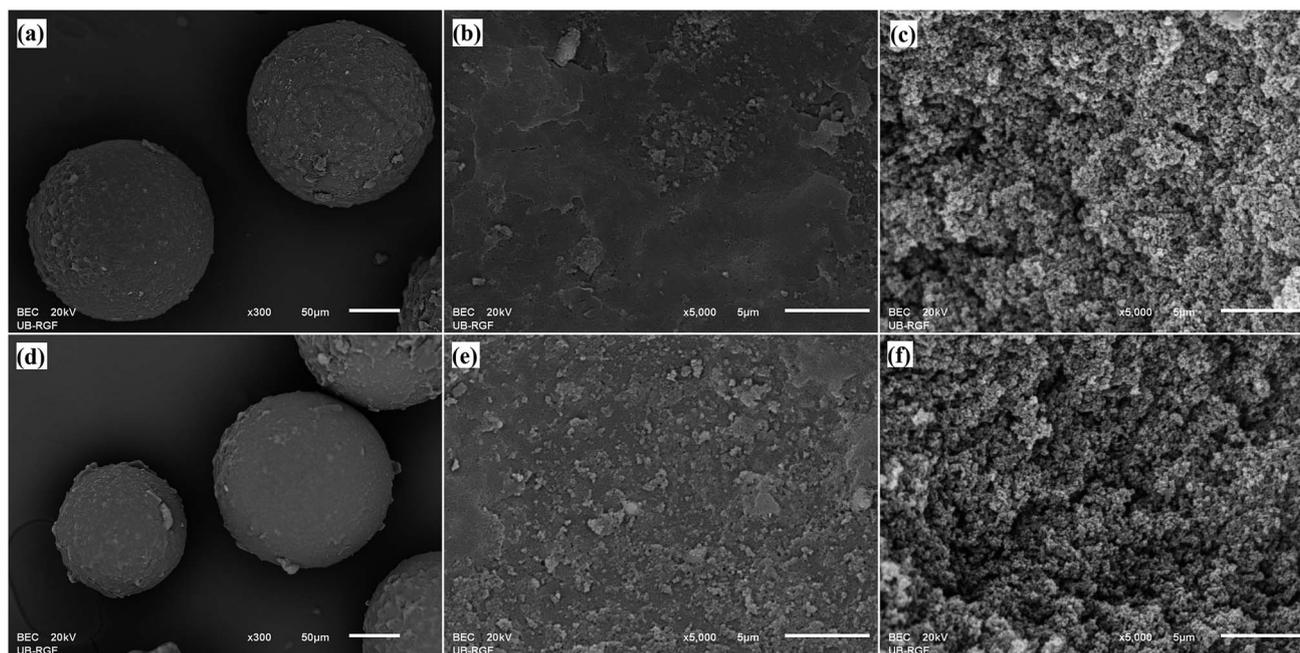
Fig. 4 SEM microphotographs of: mPGME particles (a), particle surface (b), particle cross-section (c) and mPGME–deta particles (d), particle surface (e) particle cross-section (f).

Table 3 Results of SEM-EDS analysis of mPGME and mPGME–deta particle surface and cross-section

| | Particle surface | | | | Particle cross-section | | | |
| | mPGME | | mPGME-deta | | mPGME | | mPGME-deta | |
Element	Mass%	Atomic%	Mass%	Atomic%	Mass%	Atomic%	Mass%	Atomic%
C–K	82.1	86.8	64.8	70.9	77.2	82.0	60.1	66.0
O–K	16.0	12.7	19.4	12.6	22.5	17.9	20.8	17.2
N–K	—	—	13.5	15.9	—	—	17.4	16.4
Fe–K	1.9	0.4	2.4	0.6	0.3	0.1	1.7	0.4

basic functional groups adsorb Fe(III)-containing cations[31] and magnetic copolymer obtained from suspension polymerization of styrene and divinylbenzene.[11] Highly developed internal porous structure is advantageous for the metal ions sorption due to the decrease of the mass transfer resistance, facilitation of the metal ions diffusion which consequently provides high adsorption rate and capacity.[32]

The SEM-EDS analysis confirmed the presence of all expected elements (C, O, N and Fe). The N percentage was almost the same on the particles surface and in the cross-section indicating that the reaction of epoxy groups with diethylenetriamine occurs on the surface as well as in the interior of the mPGME–deta particles. Although predominantly present at the particle surface, the iron nanoparticles were also embedded in the bulk to a certain extent.

The surface topography of mPGME and mPGME–deta was studied by atomic force microscopy (AFM). The 2D and 3D AFM images of the top view of samples mPGME and mPGME–deta are shown in Fig. 5.

A very important parameter for a potential application of the synthesized copolymers in the adsorption and ion exchange is the surface roughness.[33,34] Due to the fact that the roughness of real surfaces is hard to describe theoretically and quantitatively, the surface characterization by fractal dimension (FD) has been proved as useful.[35,36] As a measure of surface irregularity, fractal dimension varies between 2 (for a flat sample) and 3 (for an extremely rough sample).[37,38] The average roughness (R_a) and root mean square roughness (R_q) as well as fractal dimensions were presented in Table 4.

It can be noticed that mPGME surface is significantly rougher than the mPGME–deta surface as indicated by the roughness values presented in Table 4. However, the differences in fractal dimension values for mPGME and mPGME–deta are not so evident.

The magnetization curves measured for magnetite and mPGME at 300 K in a SQUID-based magnetometer in the ±5 T field range are presented in Fig. 6.
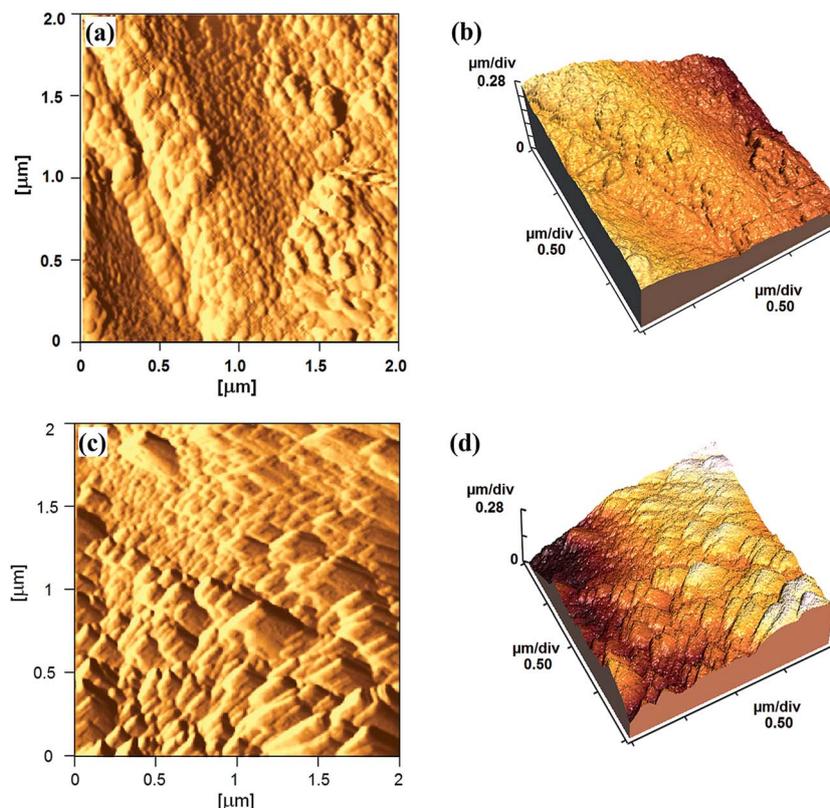
Fig. 5 The typical AFM images: (a) 2D and (b) 3D images of the mPGME; (c) 2D and (d) 3D images of the mPGME-deta.

The mPGME sample with the magnetite content of 1.4 mass% shows superparamagnetic behavior with negligible hysteresis loop. Although the saturation magnetization decreased after

Table 4 Influencing factors of textural properties of mPGME and mPGME-deta calculated using AFM data

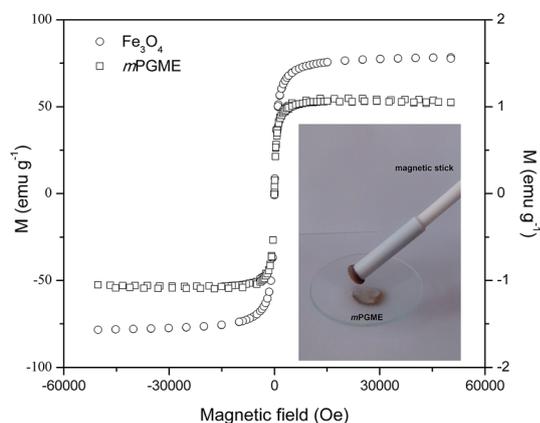| Sample	R_a, μm	R_q, nm	Fractal dimensions
mPGME	265.5	314.4	2.16
mPGME-deta	77.33	92.99	2.27

Fig. 6 Magnetic hysteresis curves of mPGME and magnetite.

magnetite incorporation in the magnetic copolymer, complete magnetic separation of mPGME was achieved by placing a magnet near the flask containing the aqueous dispersion of the magnetic copolymer particles (see Fig. 6, inset). Additional amino-functionalization had no effect on PGME magnetization. Similar was observed for silica-coated core–shell magnetite nanoparticles ($Fe_3O_4@SiO_2$) and nanoparticles with covalently grafted amino groups.[39]

The effect of contact time and pH on pertechnetate ions sorption onto mPGME-deta

The solution pH and contact time are a crucial parameters that affects the sorbent surface charge, the protonation–deprotonation of surface functional groups, metal speciation in the aqueous solution and consequently, the sorbate/sorbent interactions.[40] Thus, the influence of contact time and solution pH on TcO_4^- removal by mPGME-deta was investigated in the pH range 1.0–8.0 while keeping the other variables constant (shaking speed 120 rpm, sorbent concentration 0.2 g dm^{-3} and $T = 298$ K). The effect of the contact time (at pH 5.0) and pH (for contact time 180 min) on the removal efficiency of pertechnetate is presented in Fig. 7.

As can be seen from Fig. 7, pertechnetate ion sorption onto mPGME-deta was rather fast, with 90% and 95% of TcO_4^- sorbed within the first 5 and 30 min, respectively. In acidic medium (pH 1–3) the removal efficiency increases and then reaches the maximum of >99% in the pH range 3.0–5.0.
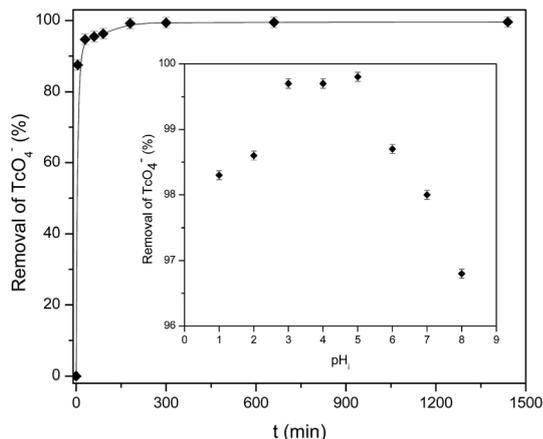
Fig. 7 Effect of contact time and pH (inset) on the sorption of pertechnetate from aqueous solution onto mPGME-deta. Vertical error bars represent standard errors.
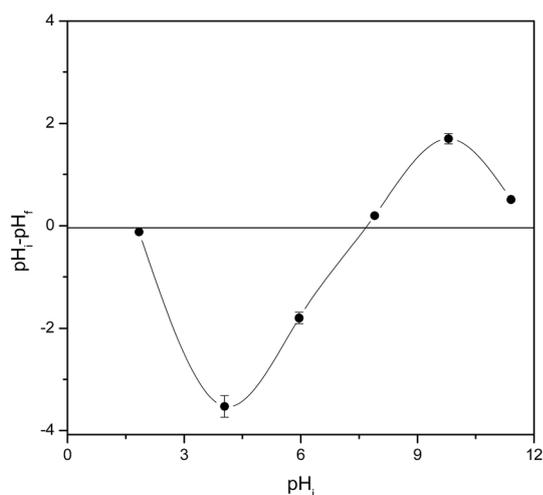

Fig. 8 Point of zero charge (pH_{pzc}) of mPGME-deta determined by the pH drift method. Standard errors are shown as vertical error bars.

With further pH increase (pH 6–8), pertechnetate sorption slightly decreased and the removal efficiency of TcO_4^- fell to 96.5%.

In order to understand the sorption mechanism, the pH values at which the surface has neutral charge (pH_{pzc}) of mPGME-deta were determined by the pH drift method. The results are shown in Fig. 8.

If the solution pH is higher than pH_{pzc}, the sorbent surface will have a negative charge and sorption of positive ions will be favored due to the electrostatic attraction. On the other hand, the sorption of negatively ions will be favored when pH < pH_{pzc}.[41] As can be seen, the pH_{pzc} for the mPGME-deta is 6.8 ± 0.3, high removal efficiency of TcO_4^- was expected to be achieved at pH below that value. Thus, in acidic medium, the electrostatic interactions between the protonated amino groups of mPGME-deta and TcO_4^- anions promote high pertechnetate removal. At pH ≥ 6, the TcO_4^- sorption decreased due to the decrease of the number of protonated amino groups in mPGME-deta.

The influence of solution pH on TcO_4^- removal by non-magnetic PGME-deta (prepared in the same manner as mPGME, in the absence of magnetite in the reaction mixture) was investigated in the pH range 3.0–7.0 and contact time of 180 min while keeping the other variables constant. The sorption performances of PGME-deta and its magnetic analogue mPGME-deta slightly differ. Namely, the removal efficiency of PGME-deta and mPGME-deta was in the range 95–98%, and 97–99%, respectively. This result was expected if one bears in mind that the TcO_4^- sorption is predominantly influenced by the surface amino groups attached to the macroporous copolymer and not the magnetization. The role of the magnetization was to enable easy and rapid separation of mPGME-deta particles from the solution after TcO_4^- sorption by an external magnetic field.

Sorption kinetics

Sorption kinetic data were analyzed using surface-reaction (PFO and PSO) and particle diffusion-based (IPD and Boyd's) kinetic models to determine the nature of sorption kinetics and the rate limiting step for pertechnetate ion were shown in Fig. 9, Tables 5 and 6.

The kinetics of pertechnetate anion sorption onto mPGME-deta is accurately described by PSO model (Fig. 9a) since the calculated q^{calc} from this model agreed very well with the experimental q^{exp} value, with high value of the correlation
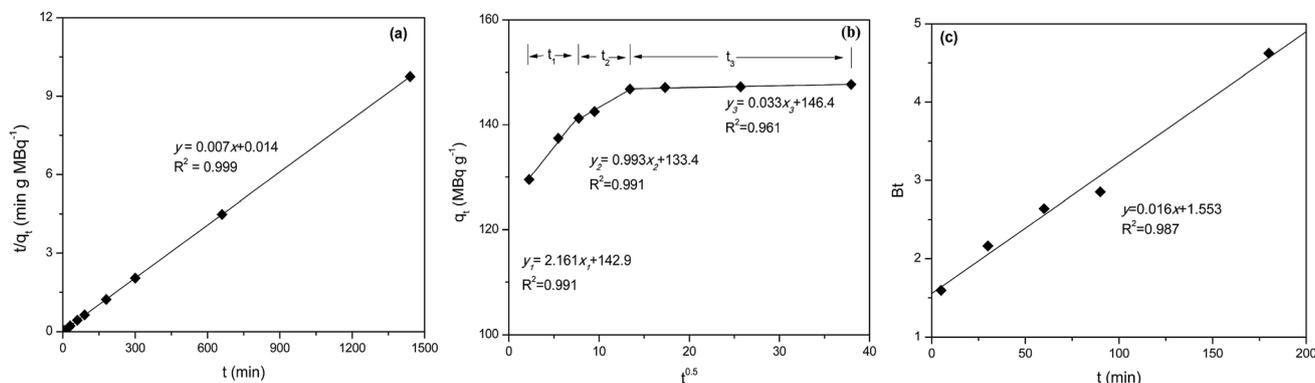

Fig. 9 Plots of PSO (a), IPD (b) and Boyd (c) kinetics model for pertechnetate ion sorption on mPGME-deta (pH = 5, t = 24 h, T = 298 K).

Table 5 Kinetic parameters for pertechnetate ion sorption using mPGME-deta (pH = 2, T = 298 K, t = 24 h)

q_e^{exp}, MBq g^{-1}	Pseudo-first-order			Pseudo-second-order		
	$k_1 \times 10^2$, min^{-1}	q_1^{calc}, MBq g^{-1}	R^2	$k_2 \times 10^3$, g MBq^{-1} min^{-1}	q_2^{calc}, MBq g^{-1}	R^2
148	1.612	19	0.987	3.50	143	0.999

Table 6 IPD parameters for TcO_4^- ion sorption using mPGME-deta (pH = 2, T = 298 K, t = 24 h)

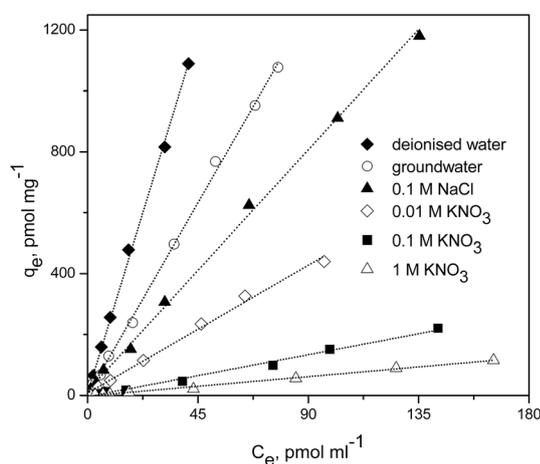| Initial linear portion			Second linear portion			Third linear portion		
k_{d1}, MBq g^{-1} min$^{-0.5}$	c_1, MBq g^{-1}	R_1^2	k_{d2}, MBq g^{-1} min$^{-0.5}$	c_2, MBq g^{-1}	R_2^2	k_{d3}, MBq g^{-1} min$^{-0.5}$	c_3, MBq g^{-1}	R_3^2
2.161	124.9	0.991	0.993	133.4	0.991	0.033	146.4	0.961

Fig. 10 Sorption isotherms of pertechnetate ion sorption on mPGME-deta from different background solutions.

coefficients (R^2 = 0.999). This implies that chemisorption mechanism plays an important role for the sorption of this anion onto mPGME-deta, *i.e.* that sorption rate is controlled by both the sorbent capacity and the sorbate concentration.

The q_t–$t^{1/2}$ plot (Fig. 9b) for IPD kinetic model applied on porous sorbents shows multi-linearity, *i.e.* has three distinct regions.[42] The first linear portion included the sorption period of 0–50 min, which represented external mass transfer and binding of pertechnetate ions sorption active sites distributed onto the outer surface of mPGME-deta. The second linear portion included the gradual sorption period of 50–250 min, representing intraparticle diffusion and binding of pertechnetate ions by active sites distributed in the mPGME-deta porous structure. The third linear portion includes the time period from 250 min to 24 h, which denoted establishment of the equilibrium. The value of c provides information about the thickness of the boundary layer, *i.e.*, the larger the intercept, the greater the boundary layer effect. From Fig. 9c it is observed that the Boyd's plot for the pertechnetate ions sorption using mPGME-deta was linear, not passing through the origin, which indicates that external mass transfer mainly governs the rate-limiting process.[43]

Adsorption isotherms

Pertechnetate ion sorption was studied on mPGME-deta at varying pertechnetate concentrations and different background solutions (at pH = 5, t = 48 h, T = 298 K). The results are presented in Fig. 10.

The reaction of TcO_4^- with mPGME-deta yielded linear adsorption isotherms, with correlation coefficients ranging from R^2 = 0.9924 to R^2 = 0.9988. The highest correlation coefficients were obtained for deionized water, groundwater and 0.1 M NaCl. The calculated values of partition coefficients, K_d, were presented in Table 7.

As can be seen from Fig. 10 and Table 7, in 0.1 M NaCl solution and in low ionic strength solution of 0.01 M KNO$_3$, TcO_4^- can be selectively and effectively removed by mPGME-deta. The observed K_d values ranged from 4679 to 8801 ml g^{-1}. When using the groundwater as a background, the K_d values were even higher, *i.e.* 14 056 ml g^{-1}. Except in a background of 0.003 M NaCl (deionized water), the TcO_4^- removal efficiency exceeded 99% and the K_d value was the highest, *i.e.* 26 360 ml g^{-1}.

The molar concentration of TcO_4^- in solution was very low (in the order of 10^{-8} to 10^{-9} M) compared to that of Cl$^-$ or NO$_3^-$ (0.01–1 M). The molar ratios of background anions to TcO_4^- ranged from 3 × 10^5 to 1 × 10^9. Under such unfavorable molar concentration ratios, TcO_4^- was highly competitive to be

**Table 7** Sorption partition coefficient for mPGME-deta in different background solutions[a]

Background solution	K_d, ml g^{-1}
Deionised water	26 360
Ground water	14 056
0.1 M NaCl	8801
0.01 M KNO$_3$	4679
0.1 M KNO$_3$	1530
1 M KNO$_3$	707

[a] It should be noted that ^{99}Mo/^{99m}Tc generator must be eluted with normal saline. So, when 0.1 ml of pertechnetate solution is added it gives 0.00308 M of NaCl in addition to background solution.

adsorbed by mPGME-deta among other mentioned anions. The NO_3^- anions appeared more effective than Cl^- in reducing TcO_4^- adsorption. In high ionic strength background solutions (0.1–1 M NaNO$_3$), the adsorption of TcO_4^- sharply decreased (Fig. 10 and Table 7).

The obtained results suggest that the main mechanism of TcO_4^- sorption onto mPGME-deta can be described by ion pair formation between NH_3^+ surface groups attached to the magnetic polymer (P) and TcO_4^- anions in solution as presented in eqn (8):

$$P\text{-}NH_3^+ + TcO_4^- \Leftrightarrow NH_3^+TcO_4^- \qquad (8)$$
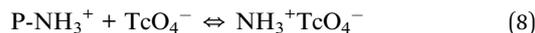
Eqn (9) describes the sorption of TcO_4^- in presence of NO_3^-:

$$P\text{-}NH_3^+ + NO_3^- \Leftrightarrow NH_3^+NO_3^- \qquad (9)$$

Although direct comparison of the reported data on pertechnetate ions sorption by different sorbents is not possible due to the different experimental conditions, some literature data will be mentioned. Previously, we investigated the removal of pertechnetate ions by using PGME-deta samples with different amount of the crosslinking monomer (EGDMA) from aqueous solutions. Linear adsorption isotherms were also found, with partitioning coefficients of 1698 ml g^{-1} and 2130 ml g^{-1}.[16] Popova et al. reported the K_d value of 3×10^5 ml g^{-1} for sorbent prepared by the noncovalent immobilization of (thia)calix[4]arenes on the Amberlite XAD-7™.[6] Bonnesen et al. used a series of monofunctional and bifunctional quaternary ammonium resins of poly(vinylbenzyl chloride)-10% divinylbenzene copolymer with various size of the trialkylammonium group for TcO_4^- uptake.[5] Monofunctional tri-n-methylammonium, tri-n-propylammonium, and tri-n-butylammonium resins showed high 24 h distribution ratios (K_d) for pertechnetate anion from groundwater test solution, i.e. 1680, 9570 and 31 800 ml g^{-1}, respectively. On the other hand, bifunctional resins containing exchange sites derived from tri-n-hexylamine in combination with either trimethylamine and triethylamine, showed higher K_d values, i.e. 13 200 and 37 300 ml g^{-1}, respectively. The K_d values for commercial strong base resins Reillex HPQ and Purolite A-520E were 4540 and 12 800 ml g^{-1}, respectively.

Conclusions

A novel magnetic macroporous mPGME sorbent has shown a strong tendency to remove pertechnetate ions (TcO_4^-) from aqueous solutions in absence and presence of competing anions. Results indicated that sorption kinetics of the pertechnetate ions on mPGME-deta was relatively fast and depends on pH and ionic strength. The amount of sorbed TcO_4^- slightly decreases with the pH decrease from 2 to 1 and pH increase from 6 to 8, indicating a lowering of the sorption capacity of mPGME-deta. We propose that non-specific sorption of pertechnetate ion via electrostatic interaction takes place at the protonated amine groups NH_3^+. The removal efficiency higher than 95% and 99% at pH 3–5 within 30 min and 180 min were

found, respectively. The pseudo-second order kinetic model fitted very well with the kinetic data of pertechnetate anion sorption onto mPGME-deta, suggesting that the sorption rate is controlled by both sorbent capacity and sorbate concentration. Particle diffusion-based models revealed the strong influence of the intraparticle diffusion and porosity of PGME-deta.

The partition coefficient (K_d) of TcO_4^- exceeded 2.6×10^4 ml g^{-1} and 1.4×10^4 ml g^{-1} when deionized water at pH 5 and groundwater were used, respectively. The sample treated with 0.1 M NaCl sorbed TcO_4^- very well at pH 5 ($K_d = 8.8 \times 10^3$ ml g^{-1}). The presence of excessive amounts of NO_3^- ions in the solution reduced the removal of TcO_4^- for 70 and 95%. The results obtained in this study suggest that mPGME-deta can be effectively used for TcO_4^- separation from aqueous solutions.

References

1 T. K. Ikäheimonen, V. P. Vartti, E. Ilus and J. Mattila, J. Radioanal. Nucl. Chem., 2002, 252, 309–313.

2 K. Shi, X. Hou, P. Roos and W. Wu, Anal. Chim. Acta, 2012, 709, 1–20.

3 Y. Wang, H. Gao, R. Yeredla, H. Xu and M. Abrecht, J. Colloid Interface Sci., 2007, 305, 209–217.

4 B. Gu, G. M. Brown, P. V. Bonnesen, L. Liang, B. A. Moyer, R. Ober and S. D. Alexandratos, Environ. Sci. Technol., 2000, 34, 1075–1080.

5 P. V. Bonnesen, G. M. Brown, S. D. Alexandratos, L. B. Bavoux, D. J. Presley, V. Patel, R. Ober and B. A. Moyer, Environ. Sci. Technol., 2000, 34, 3761–3766.

6 N. N. Popova, V. P. Morgalyuk, I. G. Tananaev, S. E. Solovieva, E. V. Popova and I. S. Antipin, Russ. Chem. Bull., 2011, 60, 175–178.

7 P. Wang, A. Khayambashi, J. Zu, Y. Wei, F. Tang and L. He, J. Radioanal. Nucl. Chem., 2016, 311, 301–306.

8 D. Horák, E. Petrovský, A. Kapička and T. Frederichs, J. Magn. Magn. Mater., 2007, 311, 500–506.

9 F. Ge, M.-M. Li, H. Ye and B.-X. Zhao, J. Hazard. Mater., 2012, 211–212, 366–372.

10 D. Horák, M. Babič, H. Macková and M. J. Beneš, J. Sep. Sci., 2007, 30, 1751–1772.

11 B. M. Conceição, M. A. S. Costa, L. C. D. S. Maria, M. R. Silva and S. H. Wang, Polimeros, 2011, 21, 409–415.

12 A. Nastasović, Z. Sandić, L. Suručić, D. Maksin, D. Jakovljević and A. Onjia, J. Hazard. Mater., 2009, 171, 153–159.

13 D. D. Maksin, A. B. Nastasović, A. D. Milutinović-Nikolić, L. T. Suručić, Z. P. Sandić, R. V. Hercigonja and A. E. Onjia, J. Hazard. Mater., 2012, 209–210, 99–110.

14 B. M. Ekmeščić, D. D. Maksin, J. P. Marković, Z. M. Vuković, R. V. Hercigonja, A. B. Nastasović and A. E. Onjia, Arabian J. Chem., 2015, DOI: 10.1016/j.arabjc.2015.11.010.

15 D. D. Maksin, R. V. Hercigonja, M. Ž. Lazarević, M. J. Žunić and A. B. Nastasović, *Polym. Bull.*, 2012, **68**, 507–528.

16 C. Guo, L. Zhou and J. Lv, *Polym. Polym. Compos.*, 2013, **21**, 449–456.

17 K. Can, M. Ozmen and M. Ersoz, *Colloids Surf., B*, 2009, **71**, 154–159.

18 L. Malović, A. Nastasović, Z. Sandić, J. Marković, D. Đorđević and Z. Vuković, *J. Mater. Sci.*, 2007, **42**, 3326–3337.

19 F. Radovanović, A. Nastasović, T. Tomković, D. Vasiljević-Radović, A. Nešić, S. Veličković and A. Onjia, *React. Funct. Polym.*, 2014, **77**, 1–10.

20 B. H. Hameed, I. A. W. Tan and A. L. Ahmad, *Chem. Eng. J.*, 2008, **144**, 235–244.

21 H. Chen, G. Dai, J. Zhao, A. Zhong, J. Wu and H. Yan, *J. Hazard. Mater.*, 2010, **177**, 228–236.

22 R. J. Kowalsky and S. Falen, *Radiopharmaceuticals in Nuclear Pharmacy and Nuclear Medicine*, American Pharmacists Association, Washington DC, USA, 2012.

23 M. Lamson 3rd, C. E. Hotte and R. D. Ice, *J. Nucl. Med. Technol.*, 1976, **4**, 21–27.

24 M. I. Khan, T. K. Min, K. Azizli, S. Sufian, H. Ullah and Z. Man, *RSC Adv.*, 2015, **5**, 61410–61420.

25 D. K. Singh, V. Kumar, V. K. Singh and S. H. Hasan, *RSC Adv.*, 2016, **6**, 56684–56697.

26 M. Žunić, A. Milutinović-Nikolić, A. Nastasović, Z. Vuković, D. Lončarević, I. Vuković, K. Loos, G. Ten Brinke and D. Jovanović, *Polym. Bull.*, 2013, **70**, 1805–1818.

27 P. A. Webb and C. Orr, *Analytical Methods in Fine Particle Technology*, Micromeritics Instrument Corp., Norcross, Georgia, United States, 1997.

28 J. Coates, in *Encyclopedia of analytical chemistry*, ed. R. A. Meyers, John Wiley and Sons Ltd, Chichester, 2006, pp. 10815–10837.

29 A. L. Andrade, D. M. Souza, M. C. Pereira, J. D. Fabris, R. Z. Domingues, U. Federal, D. M. Gerais and B. Horizonte, *Nano*, 2009, **55**, 420–424.

30 S. J. Iyengar, M. Joy, C. K. Ghosh, S. Dey, R. K. Kotnala and S. Ghosh, *RSC Adv.*, 2014, **4**, 64919–64929.

31 V. Gutsanu, C. Schitco, G. Lisa and C. Turta, *Mater. Chem. Phys.*, 2011, **130**, 853–861.

32 G. Bayramoğlu and M. Yakup Arica, *Chem. Eng. J.*, 2008, **139**, 20–28.

33 M. Raposo, Q. Ferreira and P. A. Ribeiro, in *Modern research and educational topics in microscopy*, 2007, pp. 758–769.

34 T. Silk, Q. Hong, J. Tamm and R. G. Compton, *Synth. Met.*, 1998, **93**, 65–71.

35 B. P. Radoev and B. G. Tenchov, *J. Phys. A: Math. Gen.*, 1987, **20**, L159–L162.

36 D. Avnir, D. Farin and P. Pfeifer, *J. Chem. Phys.*, 1983, **79**, 3566.

37 J. D. Miller, S. Veeramasuneni, J. Drelich, M. R. Yalamanchili and G. Yamauchi, *Polym. Eng. Sci.*, 1996, **36**, 1849–1855.

38 D. Avnir, D. Farin and P. Pfeifer, *J. Chem. Phys.*, 1983, **79**, 3566.

39 J. Wang, S. Zheng, Y. Shao, J. Liu, Z. Xu and D. Zhu, *J. Colloid Interface Sci.*, 2010, **349**, 293–299.

40 G. M. Rashad, M. R. Mahmoud, A. M. Elewa, E. Metwally and E. A. Saad, *J. Radioanal. Nucl. Chem.*, 2016, **309**, 1065–1076.

41 M. I. Kandah, R. Shawabkeh and M. A. Al-Zboon, *Appl. Surf. Sci.*, 2006, **253**, 821–826.

42 A. W. M. Ip, J. P. Barford and G. McKay, *Chem. Eng. J.*, 2010, **157**, 434–442.

43 Y. Li, Q. Wang, Q. Li, Z. Zhang, L. Zhang and X. Liu, *J. Taiwan Inst. Chem. Eng.*, 2015, **55**, 126–132.